GEOPHYSICS, VOL. 83, NO. 3 (MAY-JUNE 2018); P. 1–10, 14 FIGS.
10.1190/GEO2017-0519.1

Case History

Hockley Fault revisited: More geophysical data and new evidence on the fault location, Houston, Texas

Mustafa Saribudak[1], Michal Ruder[2], and Bob Van Nieuwenhuise[3]

ABSTRACT

Ongoing sediment deposition and related deformation in the Gulf of Mexico cause faulting in coastal areas. These faults are aseismic and underlie much of the Gulf Coast area including the city of Houston in Harris County, Texas. Considering that the average movement of these faults is approximately 8 cm per decade in Harris County, there is a great potential for structural damage to highways, utility infrastructure, and buildings that cross these features. Using integrated geophysical data, we have investigated the Hockley Fault, located in the northwest part of Harris County across Highway 290. Our magnetic, gravity, conductivity, and resistivity data displayed a fault anomaly whose location is consistent with the southern portion of the Hockley Fault mapped by previous researchers at precisely the same location. Gravity data indicate a significant fault signature that is coincident with the magnetic and conductivity data, with relatively positive gravity values observed in the downthrown section. Farther north across Highway 290, the resistivity data and the presence of fault scarps indicate that the Hockley Fault appears to be offset to the east, which has not been previously documented. The publicly available LiDAR data and historical aerial photographs of the study area support our geophysical findings. This important geohazard result impacts the mitigation plan for the Hockley Fault because it crosses and deforms Highway 290 in the study area. The nonunique model of the gravity and magnetic data indicates strong correlation of a lateral change in density and magnetic properties across the Hockley Fault. The gravity data differ from the expected signature. The high gravity observed on the downthrown side of the fault is probably caused by the compaction of unconsolidated sediments on the downthrown side. There is a narrow zone of relative negative magnetic anomalies adjacent to the fault on the downthrown side. The source of this magnetization could be due to the alteration of mineralogies by the introduction of fluids into the fault zone.

INTRODUCTION

The coastal plain of the Gulf of Mexico is underlain by a thick sequence of largely unconsolidated, lenticular deposits of clays and sands that are cut with faults (Verbeek and Clanton, 1981). These faults are primarily identified as growth faults, which are prevalent in Harris County and throughout the coastal areas of Texas and Louisiana. Growth faults are a particular type of normal fault that develops during ongoing sedimentation such that the strata on the hanging-wall side of the fault tend to be thicker than those on the footwall side (Figure 1).

Based on a study of borehole logs and seismic reflection data, faults have been delineated to depths of 3660 m below the surface (Kasmarek and Strom, 2002). The activation of these faults on the topographic surface may have resulted from natural geologic processes such as salt movement and fluid extraction (oil and gas and ground water) (Sheets, 1971; Paine, 1993). Historically, these faults have played a significant role in oil and gas exploration, and significant hydrocarbon accumulations are attributed to the presence of growth faults (Ewing, 1983; Shelton, 1984).

Since the late 1970s and early 1980s, the USGS launched an extensive fault study in the greater Houston area (Clanton and

Manuscript received by the Editor 5 August 2017; revised manuscript received 5 January 2018; published ahead of production 11 February 2018.
[1]Environmental Geophysics Associates, Austin, Texas, USA. E-mail: mbudak@pdq.net.
[2]Wintermoon Geotechnologies Inc., Glendale, Colorado, USA. E-mail: meruder@wintermoon.com.
[3]Deceased. Earth-Wave Geosciences, Houston, Texas, USA. E-mail: dvnieuwe@central.uh.edu.
© 2018 Society of Exploration Geophysicists. All rights reserved.

Amsbury, 1975; Verbeek and Clanton, 1978; Verbeek, 1979; Clanton and Verbeek, 1981; O'Neill and Van Siclen, 1984), and since then, hundreds of active faults have been identified. Today, there are more than 350 known growth faults in the Houston area.

These active faults disturb the surface in the Houston-Galveston region (Clanton and Amsbury, 1975; Clanton and Verbeek, 1981). These include the Long Point, Hockley, Addicks, Tomball, Willow Creek, and Eureka Faults (Saribudak, 2011a, 2011b). Evidence of faulting is visible from structural damage such as fractures and/or displacement of buildings, utility lines, paved roads, bridges, and railroads in the Houston area. Thus, the proper characterization and mapping of these active faults is important so that developers can avoid building in their vicinity. Furthermore, a thorough geologic understanding of these faults is critical to minimize and mitigate against their geohazard impact.

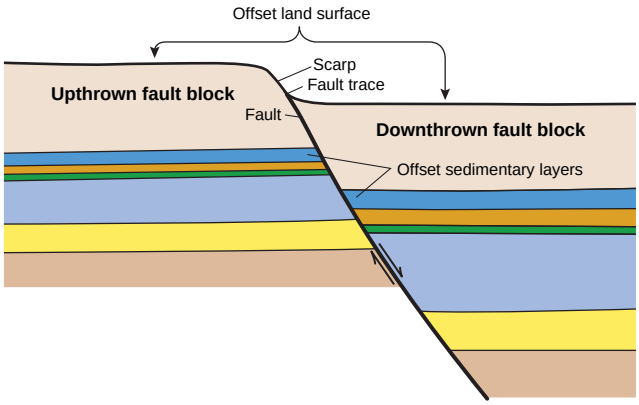

Figure 1. Diagrammatic cross section of a typical growth fault (modified from Verbeek and Clanton, 1981).

The objective of this work is to provide additional geophysical data (magnetic, conductivity, and gravity) on the Hockley Fault and to determine the accurate location of the fault across Highway 290. Figure 2 shows the Hockley Fault and the study area. The site map is taken from Khan et al. (2013), and it displays airborne LiDAR data.

GEOPHYSICAL SURVEYS OF THE HOCKLEY FAULT AT HIGHWAY 290

Seven resistivity profiles (L1–L7) and GPR data were collected across the Hockley Fault during the years 2004 and 2005 and published in Saribudak (2011a). This predated the construction of the Outlet Shopping Mall. At that time, Highway 290 consisted of two roads that were separated by a median. The locations of several scarps of the Hockley Fault were observed during this study, and these correlated well with the fault-type resistivity anomalies. Additional magnetic, gravity, and conductivity surveys of varying traverse lengths were also conducted along one of the seven resistivity profiles (L1) (see Figure 3 in Saribudak, 2011a). These data sets were unpublished until now. The locations of these geophysical profiles are shown with different colors in Figure 3. Also mapped in this figure are the locations of fault scarps and/or fault resistivity anomalies caused by the Hockley Fault across Highway 290. The site map shows the Hockley Fault trace, which crosses Highway 290, interpreted by Khan et al. (2013), using geophysical and airborne LiDAR data from 2001 and 2008, respectively.

The purpose of this research is to determine whether the Hockley Fault crosses Highway 290 as a single trace proposed by Khan et al. (2013) or in two separate offset traces, as supported by this work.

The quality of the geophysical data collected across the site was good to excellent. The traffic was light on Highway 290 during the geophysical surveys, and it did not contribute any significant noise to the geophysical data. The data acquisition was paused while a single vehicle or a group of cars appeared within 100 m of our survey location. A railroad track is located approximately 25 m to the south of profiles. There was no interference on the conductivity data due to the railroad track. The magnetic data were possibly affected by the presence of the railroad track. It should be mentioned, however, that repeated conductivity and magnetic surveys were performed along the same profile twice on different days. The general pattern of the anomalies was consistent between the data acquired on both days.

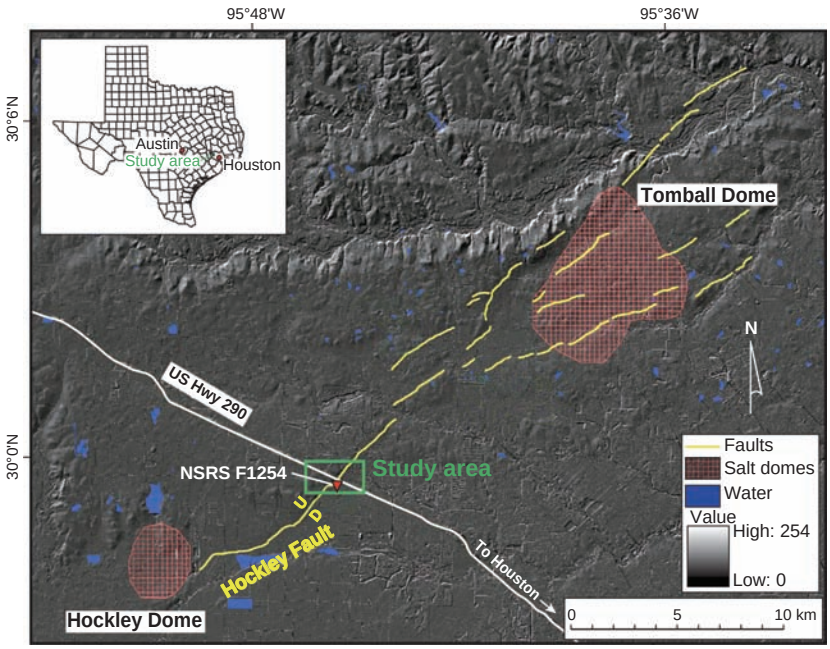

Figure 2. Site map indicating the Hockley Fault system and the geophysical study area. The map was generated by Khan et al. (2013), which shows the hillshade image generated from LiDAR data. Gray-scale units range from *x* meters to *y* meters and have been linearly scaled to 0 (dark color) and 254 (light color). Note the presence of NSRS survey marker F1254 in the downthrown section of the fault at the study area (see the "Geology" section for more information). The study area precisely corresponds to "Location One" shown by the box outlined in Khan et al. (2013)'s site map (where they performed geophysical investigation along the southern part of Highway 290.

HISTORY OF NEAR-SURFACE GEOPHYSICAL WORK OVER GROWTH FAULTS

Common methods to identify these faults include analysis of aerial photographs, field mapping, and comparison of subsurface borehole

data on the downthrown and upthrown sides of the faults, including geophysical logs and core data along with borehole data (Elsbury et al., 1980).

Pioneering resistivity work was performed over some of the Houston faults by Kreitler and McKalips (1978). They use a resistivity meter with four electrodes and conduct resistivity surveys over several fault locations using a Wenner array. Their results identified anomalous resistivity values that correlated with the locations of the faults. Years later, these resistivity results prompted one of the authors of this paper (M. Saribudak) to use a multielectrode resistivity meter and other geophysical methods (conductivity, magnetic, gravity, and GPR) across the Willow Creek growth fault. All five geophysical methods were used to map and characterize the Willow Creek Fault. All provided consistent anomalies over the fault (Saribudak and Van Nieuwenhuise, 2006). Engelkemeir and Khan (2007) publish seismic and GPR data over the Long Point Fault, which is one of the most destructive active faults in the Houston area. More resistivity surveys were conducted over the Long Point, Katy-Hockley, Tomball, and Pearland Faults, and results were published in Saribudak (2011b). During the same year, integrated geophysical results (resistivity and GPR) were published in Saribudak (2011a) for the Hockley Fault. More recently, Khan et al. (2013) publish geophysical results (seismic, gravity, and GPR), which were collected after the construction of the shopping center and expansion of Highway 290, over the Hockley Fault along with airborne LiDAR data of 2001 and 2008.

GEOLOGY OF THE HOCKLEY FAULT AT HIGHWAY 290

Figure 4 shows the general geology of the study area and stratigraphy of Harris County (Bureau of Economic Geology, 1992). In general, the Willis Formation underlies the Lissie Formation stratigraphically. Both of these Pleistocene sedimentary formations are entirely nonmarine and a series of incised stream valleys interspersed with deposits of deltas and floodplains (Ewing, 2016). The Willis Formation is composed of clays with lesser amounts of silts and sands. The Lissie Formation mainly contains sands with fewer silts and clays (Bureau of Economic Geology, 1992). According to the geologic map, the Hockley Fault lies at the contact of these two formations: on the upthrown side, the Willis Formation, and on the downthrown side, the Lissie Formation. The National Reference System (NSRS) has a survey marker on the downthrown side of the fault, which is identified as F1254. We found no specific information in the NSRS database for marker F1254 regarding the evolution of the Hockley Fault. We noted the location of this survey marker, and it is shown in all figures in this paper for georeferencing purposes. The location of the F1254 marker is 29°59′34″N latitude and 95°45′17″ west longitude.

The Hockley Fault initiates at the Hockley salt dome (Figure 2), and it trends in the northeast–southwest direction. The trend of the fault shifts to the east approximately 150 m south of Highway 290 (see the southeast location on the map in Figure 3b of Khan et al.

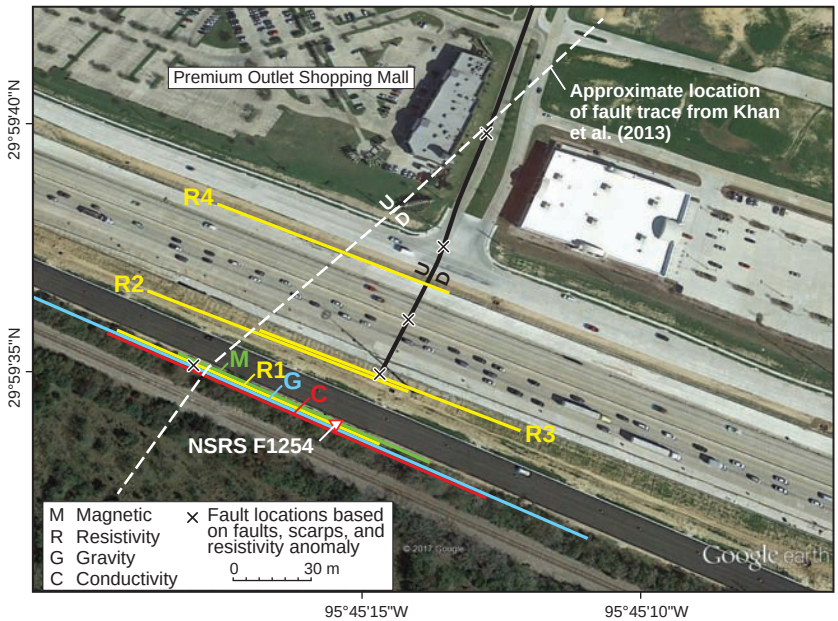

Figure 3. Site map showing the locations of magnetics (M), conductivity (C), and gravity (G) profiles. Locations of resistivity profiles (R1–R4) and fault scarps were taken from Saribudak (2011a). Note that the site map also shows the approximate trend of the Hockley Fault trace (dashed white line) interpreted by Khan et al. (2013), which obliquely crosses Highway 290.

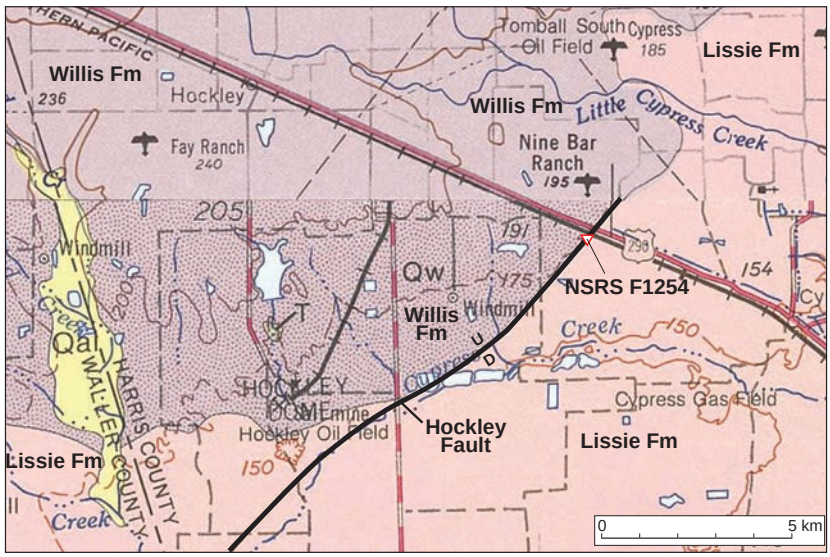

Figure 4. A geologic map of the Hockley Fault study area showing the Willis and Lissie Formations (taken from Bureau of Economic Geology, 1992). The older Willis Formation underlies the Lissie Formation. Note the location of NSRS survey marker F1254 at the Hockley Fault.

[2013] and Figure 13 in this paper). Then, the fault crosses obliquely to the north of Highway 290, adjacent to a newly built shopping center, as interpreted by Khan et al. (2013).

CONDUCTIVITY DATA

We used a Geonics EM31 conductivity meter to conduct the electromagnetic survey. The maximum depth exploration of this meter is approximately 6 m. The EM31 meter measures the apparent conductivity of soil. The data were collected in vertical dipole mode, and its unit is miliSiemen/meter (mS/m). The collection rate of the conductivity data was such that the spacing between the data points was less than 0.5 m along the profile. The length of the profile was 190 m.

Figure 5 shows the conductivity data. Conductivity values start at 27 mS/m at the west end of the profile and increase steadily to the southeast. The maximum value of 38 mS/m is attained between 65 and 100 m along the traverse and decreases to 28 mS/m with a sharp slope at the Hockley Fault and continues to fluctuate between 28 and 31 mS/m for the rest of the profile (see Figure 5). The conductivity data represent a fault-like signature over the Hockley Fault. Unconsolidated sediments with conductivity values between 27 and 38 mS/m are generally attributed to silts and sands (Kress and Teeple, 2003). These appear to be prevalent on both sides of the fault.

The NSRS survey marker F1254 is located near station 152 m (Figure 5), 52 m southeast of the fault location. The conductivity traverse overlaps a portion of the resistivity profile R1 (see Figures 3). The resistivity data show relatively low-resistivity (high conductivity) values of 24 Ωm on the upthrown side of the fault as deep as 10 m. However, relatively high-resistivity values, up to 50 Ωm (low conductivity), are imaged over the downthrown side of the fault. In fact, the conductivity values drop sharply from a 38 to 28 mS/m across the fault (Figure 5). The cause of the conductivity anomaly is likely to be the Hockley Fault.

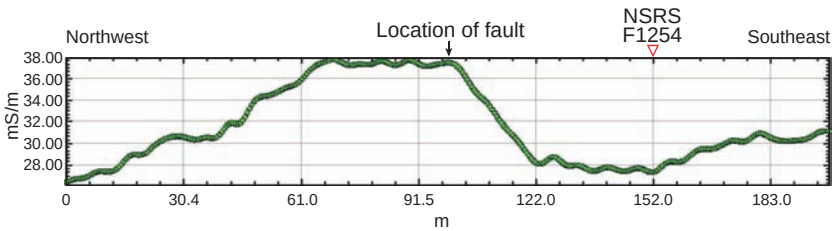

Figure 5. Conductivity anomaly indicating the location of the Hockley Fault. The location of the fault is consistent with the results of Khan et al. (2013).

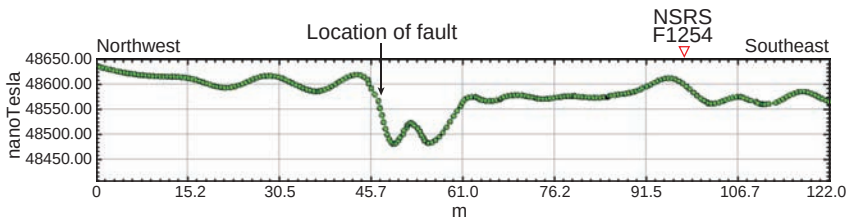

Figure 6. Magnetic anomaly indicating the location of the Hockley Fault. The magnetic expression of the fault correlates well with the conductivity data. The location of the fault is consistent with the results of Khan et al. (2013).

MAGNETIC DATA

A Geometrics G-858 Cesium magnetometer was used to acquire the data. It measures the total magnetic field in units of nT. The collection rate of the magnetic data was such that the spacing between the data points was less than 0.5 m along the magnetic profile. The length of the profile was 122 m, and the magnetic data were acquired along profile M (Figure 3). A base station was established in the vicinity of the site to record the daily variations of the earth's external magnetic field. The magnetic survey time was less than 30 min, and there were no significant diurnal variations. For this reason, a diurnal correction was not applied to the magnetic data.

A low-pass filter was applied to the magnetic data to reduce noise. The filtered profile is shown in Figure 6. The magnetic data were not reduced to pole (RTP). We advise against application of the RTP to a single profile (unless it is a truly north–south profile). For the RTP filter to properly shift the total magnetic intensity (TMI) anomaly to its correct reduced-to-pole position, 2D, or map-based information about the complete TMI dipole is required. At our survey location, TMI data along a single profile oriented northwest to southeast are not sufficient to correctly map an RTP anomaly in its proper location. The average magnetic anomaly is 48,625 nT between stations 0 and 46 m in the upthrown section of the fault. The magnetic values drop to 48,475 nT between stations 46 and 58 m, creating a significant low magnetic anomaly. The magnetic values then increase up to 48,575 nT for the rest of the profile. The magnetic profile indicates slightly more positive magnetic values on the upthrown side of the fault with respect to the downthrown side and a region of relatively low magnetic intensity in the vicinity of the fault. The source of this negative anomaly could be the alteration of magnetic minerals in the fault zone. The Willis and Lissie Formations contain iron oxide and iron-manganese nodules (Bureau of Economic Geology, 1992). The magnetic profile images a fault signature, and it is likely caused by the Hockley Fault.

It should be mentioned that a significant and well-defined relative negative magnetic anomaly was obtained over the downthrown section of the Willow Creek Fault (see Figure 7a in Saribudak and Van Nieuwenhuise, 2006), and it is very similar to the magnetic anomaly obtained over the Hockley Fault.

The locations of the Hockley Fault and the NSRS survey marker F1254 are shown as references on the profile. Their separation distance is 53 m. Note that the distances between fault locations on the conductivity and magnetic profiles and the survey marker are similar.

GRAVITY DATA

The gravity data were acquired using a LaCoste & Romberg G-Meter, SN-670. The length of the profile was 275 m. The units are in mGal.

Gravity stations were precisely located along the profile G (see Figure 3). A base station was established, and it was reoccupied three times during the survey. In addition, the data were tied to two gravity base stations: one at the Willow Creek site (Saribudak and Van Nieuwenhuise, 2006) and one at an intermediary location in Spring, Texas. This allowed for rapid reoccupation of gravity base stations and increased gravity data repeatability (<0.04 mGals) throughout the survey. The gravity station spacing was 7.5 m across the fault and 15 m away from the fault scarp.

The simple Bouguer gravity data have been referenced to the IGF1967 and the GRS1967. The data were elevation corrected using readings from a Berger/CST autolevel tied to local reference/bench marks. Microgravity data were filtered using a 7 m low-pass filter. The original gravity data were processed by the late B. Van Nieuwenhuise, and he determines the most appropriate Bouguer correction density as 2.2 g/cm^3. Unfortunately, we do not have his notes showing the acquired principal facts, his analysis, and original elevation measurements along the profile.

Gravity data, along with the topographic profile, are shown in Figure 7. The anomaly amplitude range along the profile is approximately 0.35 mGal. Gravity values range between −0.035 and −0.044 mGal in the upthrown section and steadily increase to a value of 0.18 mGal in the downthrown part of the fault. The fault location is shown at station 160 m. The distance between the start of the positive gravity anomaly and the survey marker is approximately 60 m.

There is a significant relative positive microgravity anomaly on the downthrown side of the fault. This anomaly is in contrast to the conventional gravity signature of faults. Typically, more positive gravity signatures are observed on the upthrown side of the fault, and relative negative gravity signatures are observed on the downthrown side, but this profile indicates the opposite. The elevation relief of 3 m along the gravity profile in Figure 7b does not account for the gravity anomaly observed in the downthrown section. The shape of the observed simple Bouguer anomaly does not reflect the elevation trend, indicating that the Bouguer correction has correctly removed any elevation effect that may be present in the data. We see that this "unconventional" gravity expression along the Hockley Fault is actually consistent with the gravity character across other growth faults in the region. A gravity high of similar magnitude on the downthrown side of the Willow Creek fault was obtained by Saribudak and Van Nieuwenhuise (2006). Khan et al. (2013) observe, as in this study, higher gravity values on the downthrown side of the Hockley Fault over the same location, and they label their gravity anomaly as unconventional (see Figure 7a in Khan et al., 2013).

RESISTIVITY DATA

Resistivity data (profiles R1, R2, R3, and R4) are presented in Saribudak (2011a) to emphasize an important point. Resistivity profile R1 is aligned with the conductivity, magnetic, and gravity profiles of this study and Khan et al. (2013); but the R2 and R3 profiles are located approximately 20 m to the north. Profiles R1, R2, and

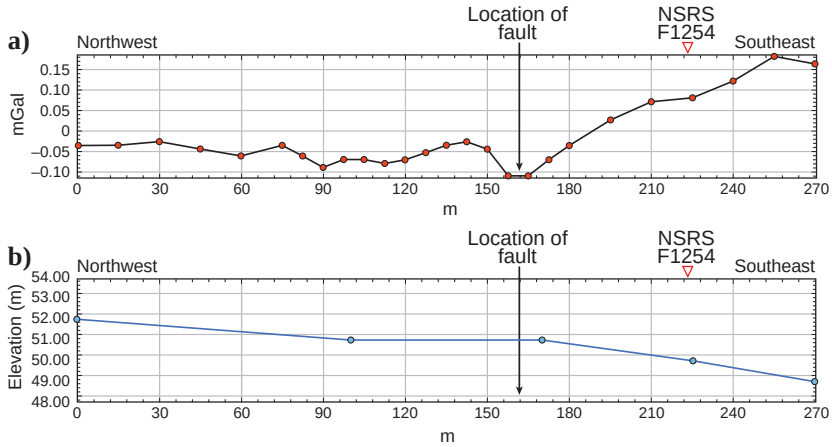

Figure 7. (a) Bouguer anomaly indicating an unconventional fault signature: higher gravity readings are observed on the downthrown side. (b) Topographic profile showing the elevation variation along the gravity profile. Location of the fault in the gravity data correlates well with its expression in the magnetic and conductivity data presented in this study and with the results of Khan et al. (2013).

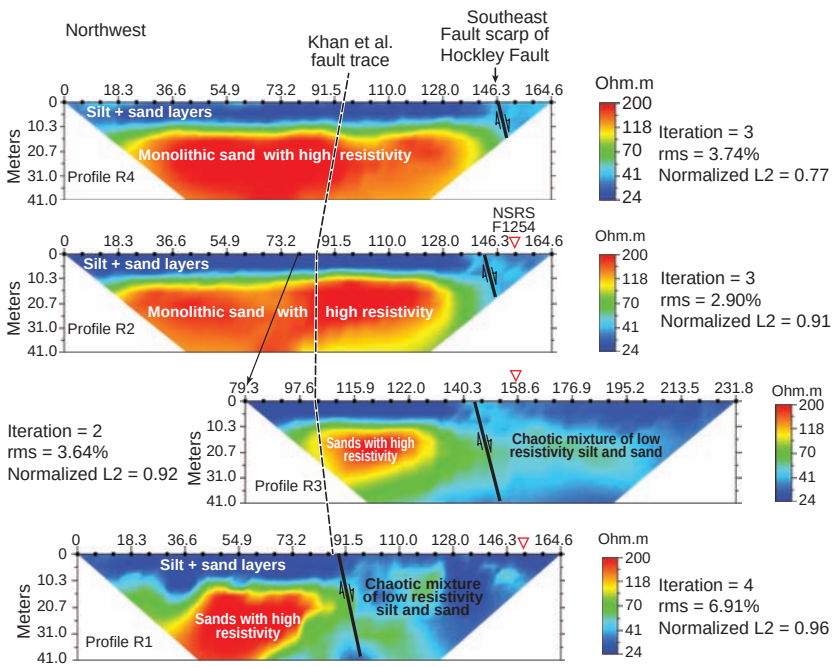

Figure 8. Resistivity data showing the fault locations and geologic units based on their resistivity values. Note that R2 and R3 are aligned along the same profile, and the latter overlaps the former. The dashed black line indicates the approximate fault trace interpreted by Khan et al. (2013). Note that there is no fault anomaly on resistivity profiles R4 and R2 in which the fault trace of Khan et al. (2013) is located.

R4 run parallel. Resistivity profile R3 overlaps profile R2 along its eastern extent (Figure 3). Note that resistivity profile R4 is located on the northern part of Highway 290 (Figure 3).

The quality of the resistivity data obtained across the site is excellent. There were no noise sources along the resistivity profiles, such as power lines and buried utility lines. The statistical values of the inverted resistivity data (L1–L4) are shown on each profile with root-mean-square (rms) and L2 (normalized) parameters, which are in the range of 3 and 7, and 0.77 and 0.96, respectively (Figure 8). These values are excellent and indicate the presence of noise-free data and reliable inversion.

Resistivity profile R1 indicates a fault-like anomaly at around station 90 m at the boundary between high- and low-resistivity units (Figure 8). In the upthrown section of the fault, relatively low-resistivity values are observed in the depth of first 5 m of the subsurface (approximately 24 Ωm), whereas in the downthrown section of the fault, relatively higher resistivity values are observed (up to 55 Ωm). This observation correlates well with the conductivity data, because the depth penetration of EM31 conductivity unit is not more than a few meters in the conductive environment. The resistivity profile displays a chaotic mixture of low-resistivity values in the downthrown section. This is probably due to the fault deformation that has taken place within the Hockley Fault zone.

This anomalous fault location correlates well with our fault locations mapped from conductivity, gravity, and magnetics and the geophysical results of Khan et al. (2013), thus corroborating a common location of the fault.

A similar fault anomaly is observed on resistivity profile R3, which is located further north of profile R1 and offset to the east by 50 m (Figure 8). The same fault-like anomaly is observed on resistivity profile R2 and R4, north across Highway 290 (see also the resistivity profiles of L5, L6, and L7 in Figures 3, 6, and 7 of Saribudak [2011a]).

Note that the fault trace (the dashed black line in Figure 8) determined by Khan et al. (2013) crosses not only resistivity profile R1, but also R2 and R4. However, our resistivity data for both the R2 and R4 traverses does not indicate the presence of any fault anomaly where Khan et al.'s. (2013) interpreted fault trace is shown (Figure 8).

The geologic map (Figure 4) shows the Willis Formation (mainly clay) on the upthrown side and the Lissie Formation (mainly sand) on the downthrown side of the Hockley Fault. The resistivity data indicate that the main lithologic unit is sand, which is observed at depths of 15–40 m. In the resistivity section, a 10 m layer of low-resistivity (clay and silt) section overlies the sand unit. Detailed review of the geologic map and the report indicates that sand units could be the channel facies of the Willis Formation (Bureau of Economic Geology, 1992).

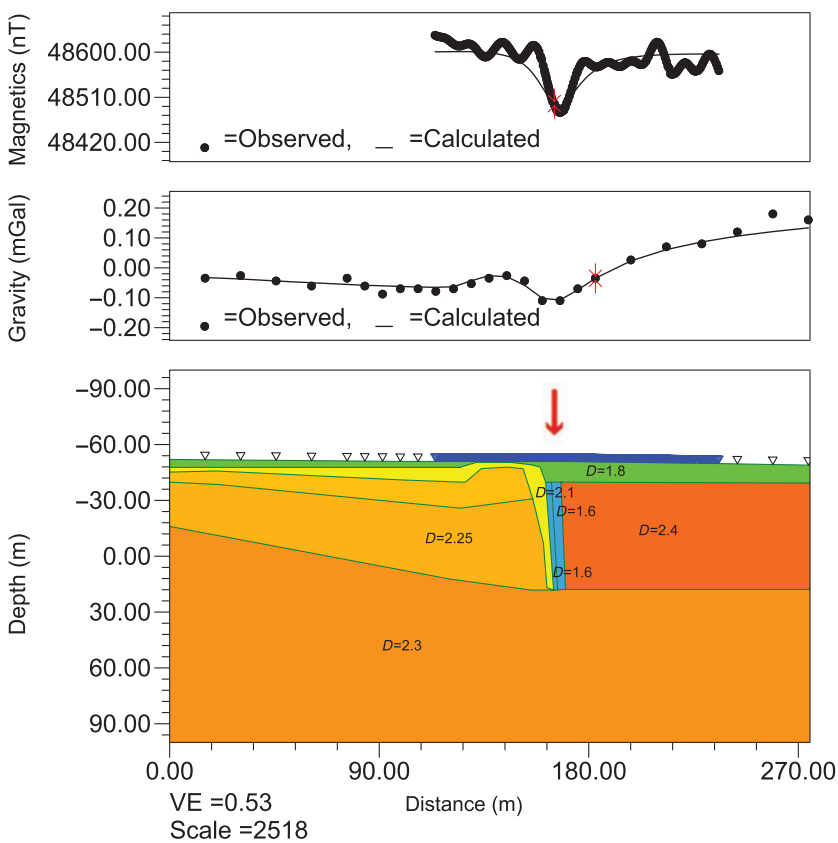

Figure 9. Modeling of gravity data. The letter *D* denotes the density of the unconsolidated sediments in the near surface. See the text for explanation. Note the presence of the low-density zone shown by the blue strip adjacent to the fault location. The red arrow indicates the location of the Hockley Fault.

GRAVITY AND MAGNETIC MODELING

Our nonunique model of the unfiltered gravity and magnetic data (Figure 9) shows a strong correlation of a lateral change in the magnetic and density properties of the Hockley Fault. The depth model, in the lower panel of Figure 9, ranges from 100 m above sea level to 100 m below sea level. The location of the fault is shown in red. The central panel shows the observed gravity and computed gravity response of the model, and the upper panel shows the observed magnetics signal and computed magnetics response of the model. The surface location of the Hockley Fault is shown as the red arrows (Figures 9 and 10).

We modeled the gravity and magnetic data using 2D forward-modeling software (Geosoft Oasis Montaj GMSYS2D). We iteratively modified the structure and physical properties (density and magnetic susceptibility) of the model until the computed response matched the observed signal. Based on resistivity modeling, we already had a general concept of the fault geometry. We used this for the structural constraint in modeling the gravity and magnetics data.

Our proposed model, color coded by density, is shown in Figure 9. It images a low-density zone of unconsolidated sediments (colored in blue) at the location of the fault. We interpreted this as a low-density fault zone, which is possibly very saturated. To the southeast, we see a high-density block of the downthrown Lissee Formation. This density (2.4) is high, considering the depth of unit; but it is possibly due to differential compaction, which is a diagenetic process that

begins during burial and may continue throughout burial and/or the duration of the growth fault. Compaction increases the bulk density and competence of rock, whereas it reduces porosity (Hooper, 1991). Compaction curves obtained from indicate that sediments whose densities are 2.0 g/cm^3 near the surface may experience an increase in their density of up to 2.6 g/cm^3 with compaction.

In addition, during our geophysical surveys at the Hockley and Willow Creek faults, we (Bob and Mustafa) observed that downthrown sides of the faults ponded rainwater for long periods of time after heavy rainfalls. We believe that the downthrown sediments were perhaps even denser than the upthrown sediments due to their saturation (https://www.engineeringtoolbox.com/dirt-mud-densities-1727.html).

Figure 10 shows the same model, color coded by magnetic susceptibility. The only magnetic source we have placed in the model is the narrow zone of anomalously magnetized material near the fault. The source of this magnetization could be due to the alteration of mineralogies by introduction of fluids into the fault zone. There is a substantial body of data regarding the importance of fault zones as conduits of vertical fluid migration in sediments (Losh et al., 1999; Kuecher et al., 2001). Evidence for growth faults as avenues of fluid migration includes fault-zone mineralization, thermal anomalies, and salinity anomalies (Hooper, 1991).

The modeled low magnetic anomaly due to the mineralized fault zone corresponds to the gravity anomaly low in density. This observation is puzzling, and we look forward to possibly observing this relationship in other fault zones.

Parameters used in the magnetic modeling are as follows: M is the magnetization of the remanence, units are micro-EMU/cm^3; S is the magnetic susceptibility, units are micro-CGS; MI is the inclination of the remanence in degrees; and MD is the declination of the remanence in degrees.

DISCUSSION

Data from four geophysical methods were used to image the Hockley Fault where it crosses Highway 290 in Cypress, Texas. The conductivity data display a typical fault anomaly with a steep slope over the fault location. The magnetic data also present a fault-like anomaly. Relatively high magnetic values are associated with the upthrown side, and relatively low magnetic values are on the downthrown side. The source of the magnetization is modeled to be the narrow zone of anomalously magnetized material near the fault location. The gravity data differ from the conventional case. A gravity high is observed on the downthrown side of the fault. It is prob-

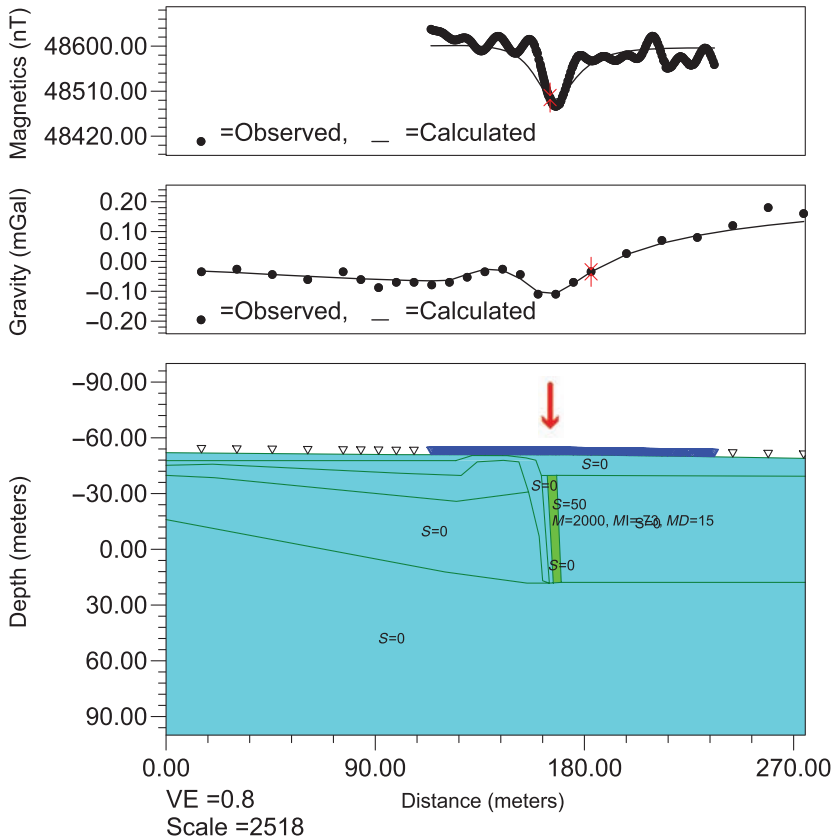

Figure 10. Modeling of magnetic data. The red arrow indicates the Hockley Fault location. The yellow strip corresponds to the low magnetic anomaly, which is interpreted to be the narrow zone of anomalously magnetized material along the fault. The magnetic data were modeled using a 10 m low-pass filter.

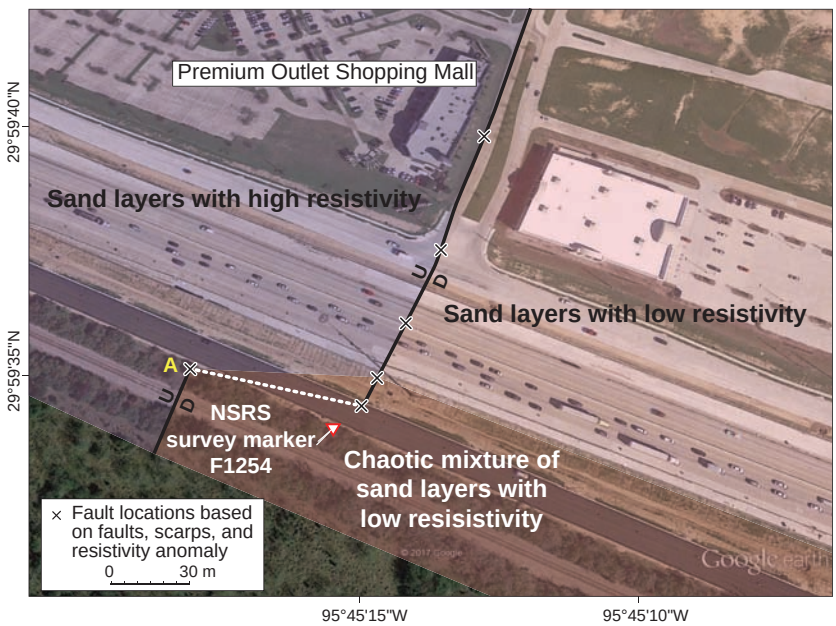

Figure 11. Schematic map showing near-surface lithologies and the shift of the Hockley Fault across Highway 290 based on the resistivity data from Saribudak (2011a) and this study. The letter A designates the location where this study and Khan et al. (2013) obtained similar fault anomalies.

ably caused by compaction and high saturation of the unconsolidated sediments in the downthrown side. We successfully model this response using slightly higher density values on the downthrown part of the fault.

Results of seismic, GPR, and gravity from Khan et al. (2013) also obtained a fault anomaly at the same location of this study. Their gravity profile indicated a similar gravity anomaly (higher readings on the downthrown side) across the Hockley Fault. It should be noted that the amplitude (approximately 0.3 mGal) and wavelength (225 m) of the fault's gravity anomaly of Khan et al. (2013) correlate well with this study, which are approximately 0.25 mGal and 270 m, respectively.

Locations of the fault based on the resistivity data (Saribudak, 2011a) and the data obtained from this study are marked on a site map (Figure 11). The common fault location determined by this study and Khan et al. (2013) is marked with a letter A (yellow color) on the southern part of Highway 290. However, fault-like anomalies obtained from the resistivity data and visible fault scarps indicate that the fault shifts to the east as it crosses north of Highway 290.

The geologic units identified by the resistivity data are also shown in Figure 11. The resistivity data in this area indicate a chaotic mixture of sand and silt units, which are probably caused by the fault zone between the two main branches of the Hockley Fault. The width of the fault zone is estimated to be approximately 65 m.

After the completion of our geophysical surveys, a shopping mall was built in the vicinity of the Hockley Fault. Highway 290 was rebuilt and extended, covering the fault outcrop. A site visit during April 2010 did not show any significant deformation across a newly built road. However, three months later, during our August 2010 site visit, we observed large cracks in the pavement along the fault trace (Figure 12).

A similar observation was noted when we studied two Google images of the study area from 2004 and 2017 (Figure 13). The 2004 image indicates a dark patch on the northern section of Highway 290. This asphalt patch covers the fault scarp and deformation on the highway at this location. However, the 2017 image did not include the patch or any related fault deformation. We precisely mapped the location of the 2004 fault patch on the 2017 Google image. In addition, we also mapped the fault trace accurately determined by Khan et al. (2013) onto the 2017 image. One can easily observe that the 2004 fault patch is located approximately 30 m to the east of the Khan et al. (2013) fault trace. Figure 13 shows the future location of the Outlet Shopping Mall and Highway 290 for reference purposes.

A 2008 LiDAR data set of the Hockley Fault area, which is publicly available, is shown in Figure 14. We show the trend of the Hockley Fault with small black and white arrows. At location A, the LiDAR data display the fault trace well on the north and south sides of Highway 290, with a visible shift, to the fault trend. However, the LiDAR data do not show any trace of the fault on Highway 290. As it appears, the trend of the fault also shifts eastward at location B on Highway 290 (Figure 14). This observation suggests that the shifting of the main Hockley Fault along its strike is an active feature. One can visit the discrete fault line and observe the ongoing fault deformation across the newly built Highway 290 as outlined in this geophysical study.

Figure 12. (a) Newly paved asphalt has been placed over the Hockley Fault in April 2010 at the entrance road of the shopping center. Note that this part of the mall was still under construction at that time; (b) the fault deformation manifested itself within three months, and cracks were patched with black asphalt.

Figure 13. Google images of 2004 and 2017: (a) A patch on the asphalt covers the fault scarp and fault deformation on Highway 290 in the year 2004; (b) the location of the 2004 patch is plotted on the 2017 Goggle image. The fault trace obtained by Khan et al. (2013) is also shown on the site map.

Figure 14. A LiDAR map showing the Hockley Fault location in the vicinity of the study area. The white and black arrows indicate the fault trace at locations A and B, respectively.

CONCLUSION

The Hockley Fault was investigated in detail with a variety of geophysical methods. Magnetic, conductivity, and gravity data imaged a fault signature across the structure in the southern portion of the study area. Two-dimensional resistivity data provided useful information for identifying the lithologies from the surface to 40 m depth. In addition, the resistivity data acquired on the south and north of Highway 290 suggest an easterly shift on the trace of the Hockley Fault. This interpretation is supported by publicly available LiDAR data and our observations of surface deformation across the study area.

New modeling of gravity and magnetic data over the fault, using resistivity models for constraint, was performed. The nonunique model of the gravity and magnetic data shows the strong correlation of a lateral change in density and magnetic properties across the Hockley Fault.

ACKNOWLEDGMENTS

Bob Van Nieuwenhuise, the coauthor of this paper, helped to collect the geophysical data during the years of 2004 and 2005. He passed away in 21 September 2014. He would have loved to have seen this paper published. He was a good friend, a colleague, and enthusiastic about his work. He loved geophysics and geology. We dedicate this work to Bob. This research project was born out of personal curiosity and was supported by the authors' financial commitment and/or their time. We thank J. Jardon, our graphic designer, who designed and drew the figures.

Special thanks to geologist A. Grubb for obtaining and delivering the LiDAR data to us and D. Van Nieuwenhuise of the University of Houston for reviewing the manuscript. Finally, we appreciate J. Paine of the Bureau of Economic Geology for his careful review of the manuscript and his insightful input.

We acknowledge the anonymous reviewers for their reviews, which greatly improved the content and flow of the paper.

REFERENCES

Bureau of Economic Geology, 1992, Geologic map of Texas: University of Texas at Austin, Virgil E. Barnes, project supervisor, Hartmann, B. M., and D. F. Scranton, cartography, scale 1:500,000.

Clanton, U. S., and D. L. Amsbury, 1975, Active faults in southeastern Harris County, Texas: Environmental Geology, **1**, 149–154, doi: 10.1007/BF02428942.

Clanton, U. S., and R. E. Verbeek, 1981, Photographic portraits of active faults in the Houston metropolitan area, Texas, *in* M. E. Etter, ed., Houston area environmental geology: Surface faulting, ground subsidence, hazard liability: Houston Geological Society, 70–113.

Elsbury, B. R., D. C. Van Siclen, and B. P. Marshall, 1980, Engineering aspects of the Houston fault problem: ASCE Fall Meeting.

Engelkemeir, R., and S. D. Khan, 2007, Near-surface geophysical studies of Houston faults: The Leading Edge, **26**, 1004–1008, doi: 10.1190/1.2769557.

Ewing, T., 2016, Texas through time: Lone star geology, landscapes and resources: Bureau of Economic Geology, Udden Series 6.

Ewing, T. E., 1983, Growth faults and salt tectonics in the Houston diaper province: Relative timing and exploration significance: Transactions of the 33rd Annual Meeting of the Gulf Coast Association of Geological Societies, 83–90.

Hooper, E. C. D., 1991, Fluid migration along growth faults in compacting sediments: Journal of Petroleum Geology, **14**, 161–180, doi: 10.1111/j.1747-5457.1991.tb00360.x.

Kasmarek, C. M., and W. E. Strom, 2002, Hydrogeology and simulation of ground-water flow and land surface subsidence in the Chicot and Evangeline aquifers, Houston, Texas: U.S. Geological Survey, Water-Resources Investigations Report 02-4022.

Khan, S. D., R. R. Stewart, M. Otoum, and L. Chang, 2013, A geophysical investigation of the active Hockley fault system near Houston, Texas: Geophysics, **78**, no. 4, B177–B185, doi: 10.1190/geo2012-0258.1.

Kreitler, C., and D. McKalips, 1978, Identification of surface faults by horizontal resistivity profiles, Texas coastal zone: Bureau of Economic Geology, Geological Circular 78-6.

Kress, H. W., and P. A. Teeple, 2003, Two-dimensional resistivity investigation of the north Cavalcade Street site, Houston, Texas: USGS Scientific Investigation Report 2005-5205.

Kuecher, G. J., S. S. Roberts, M. D. Thompson, and I. Matthews, 2001, Evidence for active growth faulting in the Terrebonne Delta Plain, South Louisiana: Implications for wetland loss and the vertical migration of petroleum, AAPG/DEG: Environmental Geosciences, **8**, 77–94, doi: 10.1046/j.1526-0984.2001.82001.x.

Losh, S., L. Eglinton, M. Schoell, and J. Wood, 1999, Vertical and lateral fluid flow related to a large growth fault, South Eugene Island Block 330 Field, offshore Louisiana: The AAPG Bulletin, **83**, 244–276.

O'Neill, M. W., and D. C. Van Siclen, 1984, Activation of Gulf Coast faults by depressuring of aquifers and an engineering approach to siting structures along their traces: Bulletin — Association of Engineering Geologists, **21**, 73–87.

Paine, J., 1993, Subsidence of the Texas coast: Inferences from historical and Late Pleistocene sea levels: Tectonophysics, **222**, 445–458, doi: 10.1016/0040-1951(93)90363-O.

Saribudak, M., 2011a, Geophysical mapping of the Hockley growth fault in northwest Houston, USA, and recent surface observations: The Leading Edge, **30**, 172–180, doi: 10.1190/1.3555328.

Saribudak, M., 2011b, 2D resistivity imaging investigation of long point, Katy-Hockley, Tomball and Pearland Faults, Houston, Texas: Houston Geological Society, **54**, 39–48.

Saribudak, M., and B. Van Nieuwenhuise, 2006, Integrated geophysical studies over an active growth fault in Houston: The Leading Edge, **25**, 332–334, doi: 10.1190/1.2184101.

Sheets, M. M., 1971, Active surface faulting in the Houston area, Texas: Houston Geological Society Bulletin, **13**, 24–33.

Shelton, J., 1984, Listric normal faults: An illustrated summary: AAPG Bulletin, **68**, 801–815.

Verbeek, E. R., 1979, Surface faults in the Gulf coastal plain between Victoria and Beaumont, Texas: Tectonophysics, **52**, 373–375, doi: 10.1016/0040-1951(79)90248-8.

Verbeek, E. R., and U. S. Clanton, 1978, Map showing faults in the southeastern Houston metropolitan area, Texas: U.S. Geological Survey Open File Report 78–79.

Verbeek, E. R., and U. S. Clanton, 1981, Historically active faults in the Houston metropolitan area, Texas, *in* M. E. Etter, ed., Houston area environmental geology: Surface faulting, ground subsidence, hazard liability: Houston Geological Society, 28–69.

View publication stats

ResearchGate

See discussions, stats, and author profiles for this publication at: https://www.researchgate.net/publication/323121001

Hockley Fault Revisited: More Geophysical Data and New Evidence on the Fault Mechanism, Houston, Texas

Article *in* Geophysics · February 2018

DOI: 10.1190/geo2017-0519.1

CITATIONS
2

READS
228

3 authors, including:

Mustafa Saribudak
Environmental Geophysics Associates (www.egatx.com)

51 PUBLICATIONS **213** CITATIONS

SEE PROFILE

Some of the authors of this publication are also working on these related projects:

Project Geophysical Imaging of the Critical Zone of Trinity/Edwards Aquifer over the Haby Fault, Balcones Fault Zone, Texas, USA View project

Project How to locate abandoned water and oil and gas wells using geophysics View project

All content following this page was uploaded by Mustafa Saribudak on 20 May 2018.

The user has requested enhancement of the downloaded file.